Locally Resonant Effective Phononic Crystals for Subwavelength Vibration Control of Torsional Cylindrical Waves

Ignacio Arretche[1]
Department of Mechanical Science and Engineering,
University of Illinois Urbana-Champaign,
1206 W. Green Street,
Urbana, IL 61801
e-mail: ia6@illinois.edu

Kathryn H. Matlack
Mem. ASME
Department of Mechanical Science and Engineering,
University of Illinois Urbana-Champaign,
1206 W. Green Street,
Urbana, IL 61801
e-mail: kmatlack@illinois.edu

Locally resonant materials allow for wave propagation control in the subwavelength regime. Even though these materials do not need periodicity, they are usually designed as periodic systems since this allows for the application of the Bloch theorem and analysis of the entire system based on a single unit cell. However, geometries that are invariant to translation result in equations of motion with periodic coefficients only if we assume plane wave propagation. When wave fronts are cylindrical or spherical, a system realized through tessellation of a unit cell does not result in periodic coefficients and the Bloch theorem cannot be applied. Therefore, most studies of periodic locally resonant systems are limited to plane wave propagation. In this article, we address this limitation by introducing a locally resonant effective phononic crystal composed of a radially varying matrix with attached torsional resonators. This material is not geometrically periodic but exhibits effective periodicity, i.e., its equations of motion are invariant to radial translations, allowing the Bloch theorem to be applied to radially propagating torsional waves. We show that this material can be analyzed under the already developed framework for metamaterials. To show the importance of using an effectively periodic system, we compare its behavior to a system that is not effectively periodic but has geometric periodicity. We show considerable differences in transmission as well as in the negative effective properties of these two systems. Locally resonant effective phononic crystals open possibilities for subwavelength elastic wave control in the near field of sources. [DOI: 10.1115/1.4052748]

Keywords: dynamics, materials in vibration and acoustics, vibration control, vibration isolation

1 Introduction

Engineered periodic materials, usually referred to as phononic crystals (PCs), allow for unprecedented ways of wave propagation control [1,2]. PCs can be designed to obtain attenuation in selective frequency ranges [3,4] or even to actively tune these ranges to adjust to external stimuli on demand [5–7]. PCs can achieve negative refraction [8], break the diffraction limit [9], and even provide robust topological wave guiding [10–13].

Since the functionality of PCs relies on the phenomenon of Bragg scattering, the wavelengths at which PCs work are closely related to the length scale of the system [14]. This becomes a limitation when trying to control waves at low frequencies because it results in impractically large systems or the need for extremely soft materials. The introduction of locally resonant materials, typically referred to as acoustic metamaterials, has provided a means of controlling waves in the subwavelength regime [15]. This not only allowed for low-frequency wave propagation control using relatively small features but also introduced other interesting phenomena such as negative effective properties [15] and enhanced damping [16].

Locally resonant materials do not need periodicity and even a single resonator can display negative effective properties [17] or provide vibration suppression [18]. However, involving periodicity in these systems allows for the application of the Bloch theorem and calculation of the band structure [14]. In this way, the behavior of the infinite system can be understood through the analysis of a single unit cell. This becomes particularly useful when dealing with complex geometries, multiple resonators, and two-dimensional (2D) and three-dimensional structures and has motivated the designs of locally resonant metamaterials to be periodic. In fact, many of the novel behaviors of locally resonant elastic metamaterials have been achieved using periodic systems. For example, negative refraction and super resolution have been achieved for square [19] and hexagonal [20,21] periodic resonator arrays, and the phenomenon of metadamping [16] was first shown for one-dimensional (1D) periodic systems.

All these studies use the Bloch theorem for analysis, and this theorem requires periodic coefficients in the equations of motion. This is why the study of periodic locally resonant materials in all the aforementioned references is limited to periodic systems with lattice vectors in a Cartesian coordinate system (or alternatively, in the far field of sources); it is for these lattice vectors that the equations of motion result in periodic coefficients when the system is geometrically periodic (i.e., geometry is invariant to translations along lattice vectors). On the contrary, when the material is invariant to translation along lattice vectors in cylindrical or spherical coordinates (or alternatively, in the near field of sources), the equations of motion that describe their behavior lack periodic coefficients and Bloch analysis cannot be applied [22–24]. In fact, most studies that deal with PCs for cylindrical waves rely on analysis of the finite structures [25–27] or far-field approximations [28,29].

When it comes to near-field vibrations, where wave fronts cannot be approximated as plane, we must appeal to other solutions to be able to apply Bloch analysis and thus utilize typical well-studied properties of local resonant systems mentioned in references herein. In this area, radial wave crystals have shown that through anisotropic radially varying material properties, the acoustic and electromagnetic equations of motion can be forced to have periodic

[1]Corresponding author.

Contributed by the Technical Committee on Vibration and Sound of ASME for publication in the Journal of Vibration and Acoustics. Manuscript received July 14, 2021; final manuscript received October 6, 2021; published online November 9, 2021. Assoc. Editor: Fabio Semperlotti.

coefficients [23], resulting in high Q-factor Fabri-Perot-like resonances. In elastic waves, the authors' recent work proposed a combination of periodic plus isotropic radially varying material properties that cause the equations of motion for radially propagating torsional waves to be equivalent to those that describe wave propagation in a Cartesian phononic material [22]. In this way, we extrapolated the typical Bloch analysis in Cartesian systems to realize band gaps and topological interface modes in cylindrical coordinates [22]. These materials are termed *effective phononic crystals* (EPCs), since, even though they are not geometrically periodic, their equations of motion effectively describe a PC. However, both radial wave crystals and EPCs are based on the Bragg scattering mechanism (with the limitations this entails) and have not included nor analyzed the effects of local resonances in the near field of sources.

In this article, we extend the concept of EPCs [22] to include local resonances in what we term a *locally resonant effective phononic crystal* (LREPC). We present a method that enables properties of Cartesian periodic locally resonant systems to be realized with cylindrical wave fronts that are present in the near field of point sources in 2D. We show that by prescribing radially varying material properties in the host medium and torsional local resonances, we can reduce the equations of motion of radial torsional waves to those of axial waves in strings [30] or bars [31] with local resonances, allowing the calculation of band structures based on methods already developed in these references. We focus here on radial torsional waves, which are relevant in rotating machinery such as turbines, compressors, and engines [32]; however, extrapolation to other polarizations can be done using an equivalent analytical treatment [22]. In fact, even though torsional vibrations are problematic in many mechanical systems, the work on locally resonant materials for torsional waves is limited to only a few studies [33,34], both of which deal with plane wave propagation in Cartesian directions (i.e., torsional waves propagating along a Cartesian axis).

To investigate LREPCs, we first construct their equations of motion by describing them as radially dependent heterogeneous material with distributed moments that account for the torsional resonators. We then use the finite element method to solve the 1D equation of motion of torsional waves propagating through a finite LREPC and calculate its transmission. We show that the behavior of the LREPC is independent of unit cell truncation and can be predicted by the analytical band structure analysis. To show the advantages of using LREPCs, we compare transmission of the finite LREPCs with that of systems that are geometrically periodic but not effectively periodic. We refer to the latter as the *homogenous system* (HS) due to its independence of material properties on radius. We present three different comparisons. For the first two, we compare using the nondimensional parameters for stiffness, moment of inertia, and frequency that are typically used for the parametric analysis of locally resonant systems [30]. We first compare transmission of the LREPC with an HS that has equivalent stiffness and moment of inertia nondimensional parameters. However, in this case, the resonators of the HS have different resonant frequencies. Thus, we construct a second comparison between an LREPC and an HS that has equal stiffness and frequency nondimensional parameters. In both of these comparisons, imposing the respective nondimensional parameters to be equal forces each of the resonators of the HS to have different stiffness and moment of inertia. Thus, we make a third comparison with an HS with resonators that are all equal and the same as those of the LREPC. Since the response of locally resonant material is strongly affected by its overall stiffness, we set the static torsional stiffness of the finite LREPC and HS to be the same in this comparison. Finally, because many of the novel wave phenomena of locally resonant systems arise from their negative effective properties [35], we calculate the ranges of negative effective dynamic moment of inertia for the LREPC and all three cases of HS. By comparing transmission and effective properties of the LREPC and the HS, we aim to show the possible advantages of using an LREPC when dealing with radial torsional waves.

2 LREPC Derivation

To derive and analyze the LREPCs, we first derive the equations of motion for a cylindrical torsional wave propagating through a heterogeneous material with varying thickness and a distributed external moment, the latter of which will ultimately capture the effects of local resonances. Assuming small tangential displacements independent of out-of-plane thickness and axisymmetric wave propagation, the global equilibrium of an infinitesimal cylindrical element (Fig. 1(*a*)) results in,

$$I\frac{\partial^2\theta(r,t)}{\partial t^2}=\frac{\partial T(r,t)}{\partial r}dr+M(r,t)dr \tag{1}$$

where θ is the angular displacement, I is the polar mass moment of inertia of the ring around its center, T is the torque on the inner ring of the infinitesimal element, and $M(r,t)$ is a distributed external moment (moment per unit radius). The torque can be expressed as follows:

$$T(r,t)=2\pi rh(r)r\sigma_{r\theta}(r,t) \tag{2}$$

where $h(r)$ is the out-of-plane thickness and $\sigma_{r\theta}$ is the shear stress. Assuming a linear isotropic material, the stresses can be written in terms of the tangential displacements as follows:

$$\begin{aligned}T(r,t)&=2\pi r^2h(r)\mu(r)\left(\frac{\partial u_\theta(r,t)}{\partial r}-\frac{u_\theta(r,t)}{r}\right)\\&=2\pi r^3h(r)\mu(r)\frac{\partial\theta(r,t)}{\partial r}\end{aligned} \tag{3}$$

where $\mu(r)$ is the material shear modulus and $u_\theta=r\theta$ is the tangential displacement. Given that the polar mass moment of inertia of the infinitesimal ring is

$$I=\rho(r)(2\pi rdr)h(r)r^2 \tag{4}$$

we can combine Eqs. (1), (3), and (4) to obtain the equations of motion for radially propagating torsional waves,

$$2\pi r^3\rho(r)h(r)\frac{\partial^2\theta(r,t)}{\partial t^2}=\frac{\partial}{\partial r}\left(2\pi r^3\mu(r)h(r)\frac{\partial\theta(r,t)}{\partial r}\right)+M(r,t) \tag{5}$$

We add an infinite set of resonators of equal torsional stiffness, β_r, and equal polar mass moment of inertia, I_r, periodically spaced a distance Δr from each other (Fig. 1(*b*)) to Eq. (5), by considering them as moments distributed along an infinitesimal ring and adding an extra degree-of-freedom per resonator. Thus, the set of equations that describes this system is

$$\begin{cases}r^3B(r)\dfrac{\partial^2\theta(r,t)}{\partial t^2}=\dfrac{\partial}{\partial r}\left(r^3A(r)\dfrac{\partial\theta}{\partial r}\right)+\displaystyle\sum_i\beta_r(\theta(r_i,t)-\theta_i(t))\delta(r-r_i)\\ I_r\dfrac{d^2\theta_i(t)}{dt^2}=\beta_r(\theta_i(t)-\theta(r_i,t))\end{cases} \tag{6}$$

where $B(r)=2\pi\rho(r)h(r)$ is the matrix density function, $A(r)=2\pi\mu(r)h(r)$ is the matrix stiffness function, $\delta(r)$ is the Kronecker-Delta function, θ_i is the angular displacement of resonator i, $r_i=r_0+i\Delta r$ is the location of resonator i, and r_0 is the internal radius (Fig. 1(*d*)). Note that μ, ρ, and h are the shear modulus, density, and out-of-plane thickness of the material to which the resonators are attached (light gray in Fig. 1), and they are assumed to be a function of the radius. For the remainder of this article, we refer to the material to which resonators are attached as the *matrix*.

Inspection of Eq. (6) shows that periodic material properties and/or thicknesses (i.e., periodic $A(r)$ and $B(r)$) do not yield equations with periodic coefficients. Neither will we have periodic coefficients if the material properties and thickness of the matrix are constant. This is different from the case of plane waves in for example strings [30], bars [31], beams [36], shafts [34], or plates [37] with local resonances. Generally, the Bloch theorem in our case cannot

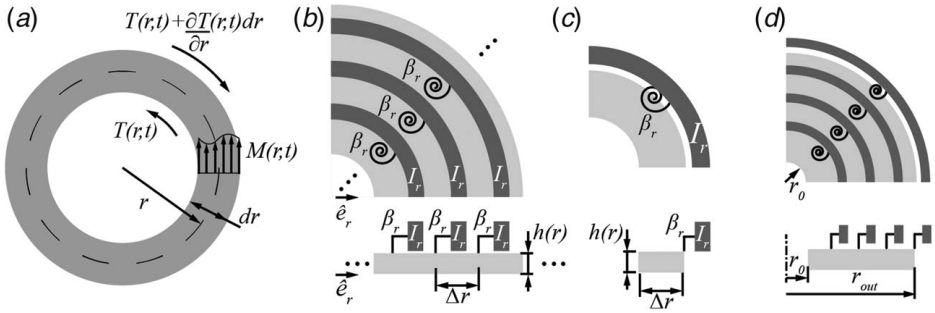

Fig. 1 (*a*) Infinitesimal radial element with a distributed moment, (*b*) infinite LREPC with local torsional resonances, (c) LREPC unit cell, and (*d*) finite four-unit cell LREPC with local resonances

be applied, and the analysis used in these references becomes invalid unless we find a way to force periodic coefficients in the equations of motion. Thus, we define $A(r)$ and $B(r)$ not to be periodic or constant, but to be such that the equations of motion are periodic. We can do this by setting,

$$\begin{cases} A(r) = \dfrac{A_0}{r^3} \\ B(r) = \dfrac{B_0}{r^3} \end{cases} \tag{7}$$

where A_0 and B_0 are constants that scale the stiffness and density, respectively, of the underlying media in the LREPC. Essentially, to physically realize the LREPC, the products of the matrix modulus and the matrix density with its thickness must be inversely proportional to r^3. For example, one way of physical realization is to have a matrix made of a homogenous material and vary its thickness with r^{-3}. The equations of motion for this selection of $A(r)$ and $B(r)$ reduce to

$$\begin{cases} B_0 \dfrac{\partial^2 \theta(r,\, t)}{\partial t^2} = A_0 \dfrac{\partial^2 \theta}{\partial r^2} + \displaystyle\sum_i \beta_r(\theta(r_i,\, t) - \theta_i(t))\delta(r - r_i) \\ I_r \dfrac{d^2\theta_i(t)}{dt^2} = \beta_r(\theta_i(t) - \theta(r_i,\, t)) \end{cases} \tag{8}$$

These equations are now invariant to translations of the form $r \to r + i\Delta r$, and thus, we can apply the Bloch theorem. In fact, these equations are equivalent to those of the systems in Refs. [30,31,34,36], and thus, analysis therein is valid here as well without parametric limitations. Note that the system we have developed does not have *geometric* periodicity (i.e., we cannot translate a unit cell along its radial lattice vector to recover the full system), but its equations of motion have periodic coefficients, and thus, its behavior will mimic that of a Cartesian geometrically periodic system. This system is effectively periodic and contains local resonances, and thus, we refer to it as a LREPC.

The analysis of LREPCs is straightforward, since their equations of motion are equivalent to the well-known one-dimensional Cartesian system with periodic local resonances. The dispersion relation for this system can be obtained by applying the Bloch theorem using an LREPC unit cell (Fig. 1(*c*)) [30]:

$$\cos(k\Delta r) = \cos(\kappa\Delta r) - \frac{P}{2}\sin(\kappa\Delta r) \tag{9}$$

where k is the Bloch wave number, $\kappa = \omega\sqrt{\dfrac{B_0}{A_0}}$, and $P = \dfrac{\omega^2 I_r \beta_r}{A_0\kappa(\beta_r - \omega^2 I_r)}$. Here, the definition of the unit cell is strictly mathematical and in terms of the equations of motion. We define the unit cell of the LREPC as the geometry that when tessellated in space by its lattice vectors (in this case, $\Delta r\hat{e}_r$; see Fig. 1(*b*)), keeps its equations of motion invariant. This is different from the typical geometrical definition of unit cell, where tessellation of the unit cell results in the entire geometry. Following the normalization given in Ref. [30], we define the following set of nondimensional parameters for the LREPC,

$$\bar{I}_{\text{LREPC}} = \frac{I_r}{B_0\Delta r} \tag{10}$$

$$\bar{\beta}_{\text{LREPC}} = \frac{\beta_r \Delta r}{A_0} \tag{11}$$

$$\bar{\omega}_{\text{LREPC}} = \frac{\omega_r}{\omega_0} \tag{12}$$

where $\omega_0 = \dfrac{\pi}{\Delta r}\sqrt{\dfrac{A_0}{B_0}}$ is the Bragg frequency associated with the unit cell and the overbar indicates a nondimensional parameter. Note that the quasi-static torsional stiffness of the matrix material of a unit cell of the LREPC is $\beta_{m_{\text{LREPC}}} = \dfrac{A_0}{\Delta r}$ and its moment of inertia $I_{m_{\text{LREPC}}} = B_0\Delta r$ (see Appendices A and B for the calculation of stiffness and inertia of the matrix). Thus, we can interpret Eqs. (10) and (11) as inertia and stiffness ratios of resonators to the matrix material, respectively. The dispersion relation can then be written in terms of these nondimensional quantities as follows:

$$\cos(k\Delta r) = \cos\left(\frac{\omega}{\omega_0}\pi\right) - \frac{Q}{2}\sin\left(\frac{\omega}{\omega_0}\pi\right) \tag{13}$$

where $Q = \dfrac{\bar{I}_{\text{LREPC}}\pi\bar{\omega}^2_{\text{LREPC}}(\omega/\omega_0)}{\bar{\omega}^2_{\text{LREPC}} - (\omega/\omega_0)^2}$. Note that $\bar{\beta}_{\text{LREPC}}$ does not appear in this expression for the dispersion relation because only two of the three nondimensional parameters in Eqs. (10)–(12) are independent. For example, algebraic manipulation results in $\bar{\omega}_{\text{LREPC}} = \dfrac{1}{\pi}\sqrt{\dfrac{\bar{\beta}_{\text{LREPC}}}{\bar{I}_{\text{LREPC}}}}$, and we could rewrite Eq. (13) in terms of $\bar{\beta}_{\text{LREPC}}$ instead of $\bar{I}_{\text{LREPC}}$. We introduce all three of these parameters because they will later become useful when comparing the LREPC with a noneffectively periodic system.

3 Comparisons Between LREPCs and Homogenous Systems

To understand the advantages of using an LREPC, particularly when it comes to near-field vibrations, we compare it to a material whose matrix consists of constants μ, ρ, and h (Eq. (6)):

$$\begin{cases} A_{\text{HS}}(r) = A_{0_{\text{HS}}} \\ B_{\text{HS}}(r) = B_{0_{\text{HS}}} \end{cases} \tag{14}$$

where $A_{0_{\text{HS}}}$ and $B_{0_{\text{HS}}}$ are stiffness and density constants, respectively. We refer to this system as the HS. The HS has material properties that are independent of radius, and thus, we can define a unit cell in the HS that results in the entire geometry when tessellated

along the radial lattice vector, $\Delta r\hat{e}_r$ (Fig. 1(*c*) with constant h and matrix material properties). In this way, we can say the HS is a *geometrically* periodic system. However, this system does not have periodic coefficients in the equations of motion (Eq. (6)) and cannot be analyzed using the Bloch theorem, and therefore, it is not *effectively* periodic. Thus, it is not possible to obtain the behavior of the HS based on a unit cell analysis and the response of the finite HS will depend on how we decide to truncate the system [22]. To compare the LREPC to the HS, we must do so in terms of the response of their finite versions. Therefore, we compare the LREPC and the HS by calculating the transmission of a four-unit cell system (Fig. 1(*d*)) for different ratios of internal radius (r_0) to periodicity constant (Δr). We choose four-unit cells because (1) typical periodic systems approximate the infinite behavior predicted from the band structure and we expect a four-unit cell LREPC behavior to have enough units to approximate the band structure prediction and (2) when using a limited number of unit cells, most of the system remains in the near field, where effective periodicity becomes most important. We use a 1D finite element code programmed in MATLAB to solve for the frequency response of the finite systems (Eq. (6)) assuming material properties of Eqs. (7) and (14), for the LREPC and HS, respectively. We calculate transmission as the ratio of input to output angular displacements.

In locally resonant systems, the behavior is strongly influenced by how stiff and dense the matrix material is compared to the stiffness and moment of inertia of the resonators (Eqs. (10)–(13)). Thus, a fair comparison between LREPCs and HS is one where the relationship between stiffness and moment of inertia of the matrix materials and those of the resonators of the two systems are somehow comparable. We can do this by using two different approaches: (1) define a set of nondimensional parameters in Eqs. (10)–(12) for the HS and compare the LREPC to the HS with equal nondimensional parameters and (2) compare the LREPC and HS with equal torsional static stiffness and equal resonators. For all cases, we calculate the transmission for different internal radii to periodicity constant ratios, $r_0/\Delta r$ (Fig. 1(*d*)). The purpose of these case studies is to show that the LREPC response is different than the HS in the near field, i.e., at small $r_0/\Delta r$, and gradually converges to the HS in the far field, i.e., as $r_0/\Delta r$ increases.

3.1 Comparison Between LREPC and Homogenous System Based on Stiffness, Mass, and Frequency Ratios. To compare the LREPC and HS with equal nondimensional parameters, we first define these parameters for the HS. Equations (10) and (11) can be interpreted in terms of resonator to matrix stiffness and inertia ratios, respectively. Thus, we define the stiffness and inertia nondimensional parameters of the HS based on this interpretation.

$$\bar{\beta}_{\mathrm{HS}} = \frac{\beta_r}{\beta_{m_{\mathrm{HS}}}} = \frac{\beta_r}{2A_{0_{\mathrm{HS}}}\left(\dfrac{r_2^2 r_1^2}{r_2^2 - r_1^2}\right)} \tag{15}$$

$$\bar{I}_{\mathrm{HS}} = \frac{I_r}{I_{m_{\mathrm{HS}}}} = \frac{I_r}{\dfrac{B_{0_{\mathrm{HS}}}}{4}(r_2^4 - r_1^4)} \tag{16}$$

where $\beta_{m_{\mathrm{HS}}}$ and $I_{m_{\mathrm{HS}}}$ are quasi-static torsional stiffness and inertia of the unit cell of the matrix of the HS (see Appendices A and B for further details), $r_1 = r_0 + (n-1)\Delta r$ and $r_2 = r_0 + n\Delta r$, where n is the unit cell number. Finally, for $\bar{\omega}$, we define an analogous ω_0 based on the matrix material properties,

$$\bar{\omega}_{\mathrm{HS}} = \frac{\omega_r}{\omega_{0_{\mathrm{HS}}}} = \frac{\omega_r}{\dfrac{\pi}{\Delta r}\sqrt{\dfrac{A_{0_{\mathrm{HS}}}}{B_{0_{\mathrm{HS}}}}}}} \tag{17}$$

Note that $\omega_{0_{\mathrm{HS}}}$ is not the Bragg frequency of the HS, but it is defined in an analogous way as ω_0. In fact, a Bragg frequency does not exist for the HS since it is not effectively periodic. Both $\bar{\beta}_{\mathrm{HS}}$ and $\bar{I}_{\mathrm{HS}}$ are dependent on the radial location of the unit cell. This is a direct result of the material not being effectively periodic. Furthermore, they each have a different dependence on radius. Thus, forcing these two parameters to be the same in all units changes the resonance frequencies of the resonators, resulting in different $\bar{\omega}_{\mathrm{HS}}$ for each unit cell. Similarly, if we fix $\bar{\omega}_{\mathrm{HS}}$ and $\bar{\beta}_{\mathrm{HS}}$(or $\bar{I}_{\mathrm{HS}}$) to be the same in all units, then $\bar{I}_{\mathrm{HS}}$ (or $\bar{\beta}_{\mathrm{HS}}$) will vary. In summary, only two of these three parameters can be fixed to be equal to those in the LREPC in all units, and the other one must be allowed to vary.

Here, we analyze two cases: one where $\bar{\beta}_{\mathrm{HS}}$ and $\bar{I}_{\mathrm{HS}}$ are fixed to be equal to those of the LREPC and $\bar{\omega}_{\mathrm{HS}}$ is allowed to vary, and one where $\bar{\beta}_{\mathrm{HS}}$ and $\bar{\omega}_{\mathrm{HS}}$ are fixed to be equal to those of the LREPC and $\bar{I}_{\mathrm{HS}}$ is allowed to vary. Fixing $\bar{I}_{\mathrm{HS}}$ and $\bar{\omega}_{\mathrm{HS}}$ has an analogous result to fixing $\bar{\beta}_{\mathrm{HS}}$ and $\bar{\omega}_{\mathrm{HS}}$, and thus, we exclude it from this article since it does not add any further understanding. For all comparisons, we keep the shear wave speed of the matrix the same in the LREPC and HS $\left(\text{i.e., } \dfrac{A_0}{B_0} = \dfrac{A_{0_{\mathrm{HS}}}}{B_{0_{\mathrm{HS}}}}\right)$, and thus, $\omega_{0_{\mathrm{HS}}} = \omega_0$.

3.1.1 $\bar{\boldsymbol{\beta}}_{\mathrm{LREPC}} = \bar{\boldsymbol{\beta}}_{\mathrm{HS}}$ *and* $\bar{\boldsymbol{I}}_{\mathrm{LREPC}} = \bar{\boldsymbol{I}}_{\mathrm{HS}}$. We first impose $\bar{\beta}_{\mathrm{LREPC}} = \bar{\beta}_{\mathrm{HS}}$ and $\bar{I}_{\mathrm{LREPC}} = \bar{I}_{\mathrm{HS}}$ in all units. To see the effect these constants have on the LREPC and HS systems, we calculate the band structure of the LREPC, $\bar{\omega}$, and transmission for both the LREPC and HS for different values of $\bar{\beta}_{\mathrm{LREPC}}$ and $\bar{I}_{\mathrm{LREPC}}$ (Fig. 2).

Forcing stiffness and inertia parameters to be equal in the LREPC and HS imposes $\bar{\omega}_{\mathrm{HS}} \neq \bar{\omega}_{\mathrm{LREPC}}$, which is more pronounced at smaller $r_0/\Delta r$ (Fig. 2(*b*)). Furthermore, $\bar{\omega}_{\mathrm{HS}} \to \bar{\omega}_{\mathrm{LREPC}}$ as the unit cell number increases (Fig. 2(*b*)). Thus, the behavior of the last few units of the HS should approach those of the LREPC. This will affect the effective dynamic moment of inertias of each unit cell of the HS (Sec. 4).

As $r_0/\Delta r$ increases, $\dfrac{\bar{\beta}_{\mathrm{HS}}}{\bar{I}_{\mathrm{HS}}} \to \dfrac{\bar{\beta}_{\mathrm{LREPC}}}{\bar{I}_{\mathrm{LREPC}}}$ and the resonator resonances of the HS converge to those of the LREPC (Fig. 2(*b*)). Thus, the transmission response of the HS approaches that of the LREPC (Figs. 2(*c*) and 2(*d*)). This is analogous to the far field of sources where waves are approximately plane.

Transmission reduction of the LREPC (Figs. 2(*c*) and 2(*d*)) agrees well with the predicted band gaps from dispersion (Fig. 2(*a*)) for all $\bar{\beta}_{\mathrm{LREPC}}$ and $\bar{I}_{\mathrm{LREPC}}$. As expected, as these nondimensional parameters increase, the band gap width increases (Fig. 2(*a*)), which is also reflected in the transmission curves (Fig. 2(*c*)). We do not include the response of the LREPC for different $r_0/\Delta r$ in Figs. 2(*c*) and 2(*d*) because the response of the LREPC is independent of this ratio since it is effectively periodic. The varying material properties of the LREPC compensate for diffraction typical of cylindrical waves, and thus, we see no reduction in transmission outside the band gap region. Essentially, radial torsional waves in the LREPC behave as plane waves, and thus, they do not show fundamental features of cylindrical waves such as complex acoustic impedance or spatial wave attenuation from diffraction in the nondissipative system. The response of the LREPC to torsional waves is equivalent to that of a Cartesian system with periodic local resonances. Therefore, any properties of metamaterials that exist through periodic assumptions and band structure analysis apply to the LREPC in the near and far fields.

The behavior of the HS, on the other hand, strongly depends on $r_0/\Delta r$. In fact, the response of this system is quite different from that of the LRPEC in the near field, i.e., small $r_0/\Delta r$, for all $\bar{\beta}$ and $\bar{I}$ (Figs. 2(*c*) and 2(*d*)). The detuning of resonators of the different unit cells (Fig. 2(*b*)) results in a reduction in transmission that is not aligned with the band gap predicted by the dispersion curve of the LREPC. In fact, peaks followed by narrow dips are present in the lower frequency range (Fig. 2(*c*)). These dips widen as the inertia and stiffness ratios increase (Figs. 2(ci)–2(ciii)) due to the larger resonator masses. Interestingly, at large $\bar{\beta}$ and $\bar{I}$, these peaks and dips widen such that they overlap for the last three resonators (Fig. 2(*d*iii)), resulting in a rainbow-trapping like effect [38].

The reason for the differences found in this comparison is that the HS does not have the same resonance frequency in all its resonators.

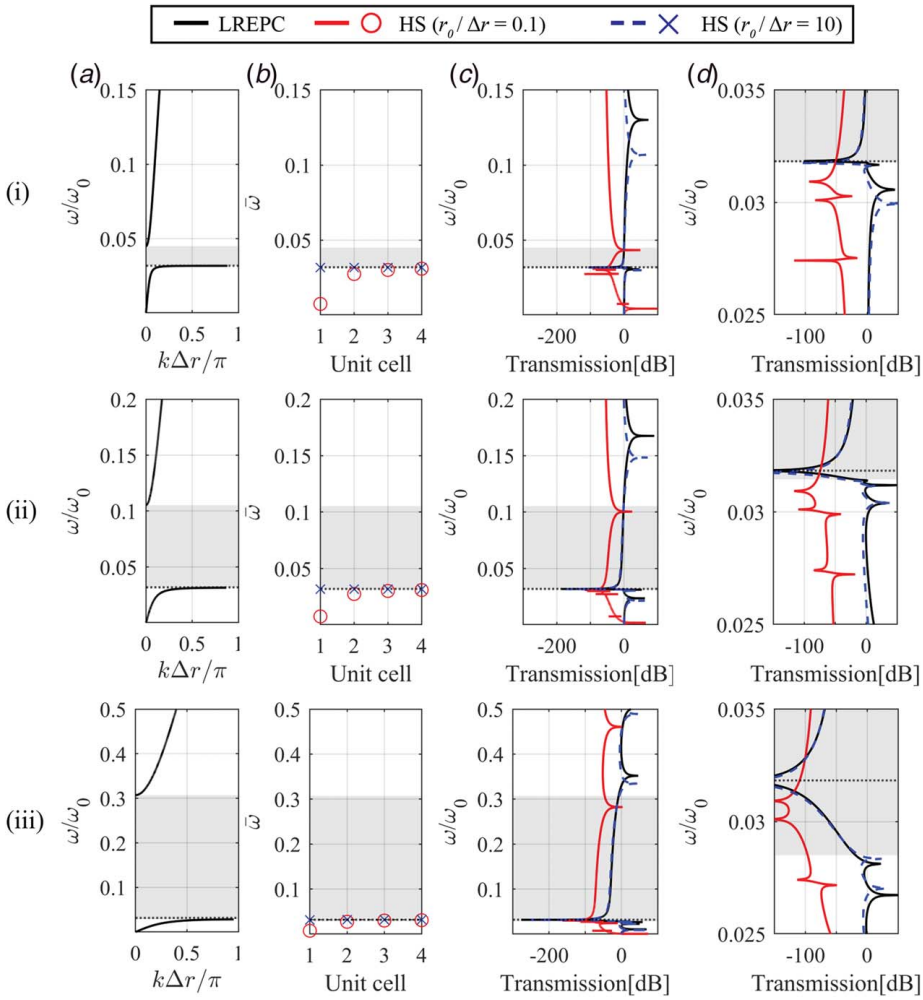

Fig. 2 (*a*) LREPC band structure, (*b*) dependence of $\bar{\omega}$ on unit cell, (*c*) transmission, and (*d*) zoom in of transmission close to the lower band gap edge of the LREPC. Parameters for each row are as follows: (i) $\bar{\beta}_{\text{LREPC}} = \bar{\beta}_{\text{HS}} = 0.01$ and $\bar{I}_{\text{LREPC}} = \bar{I}_{\text{HS}} = 1$, (ii) $\bar{\beta}_{\text{LREPC}} = \bar{\beta}_{\text{HS}} = 0.1$ and $\bar{I}_{\text{LREPC}} = \bar{I}_{\text{HS}} = 10$, and (iii) $\bar{\beta}_{\text{LREPC}} = \bar{\beta}_{\text{HS}} = 1$ and $\bar{I}_{\text{LREPC}} = \bar{I}_{\text{HS}} = 100$. Black-dotted lines indicate the resonance frequency of the LRPEC resonators.

The lack of effective periodicity of the HS system forces the resonant frequencies of each of its resonators to be different enough to considerably affect the response when keeping $\bar{\beta}$ and $\bar{I}$ constant across its units.

3.1.2 $\bar{\beta}_{\text{LREPC}} = \bar{\beta}_{\text{HS}}$ *and* $\bar{\omega}_{\text{LREPC}} = \bar{\omega}_{\text{HS}}$. In this next case, we set $\bar{\beta}_{\text{HS}} = \bar{\beta}_{\text{LREPC}}$ and $\bar{\omega}_{\text{HS}} = \bar{\omega}_{\text{LREPC}}$ to understand what happens when the resonance frequencies of resonators are all the same in the HS. Note that since $\bar{\omega}_{\text{HS}}$ is constant, all resonators of the HS have the same resonance frequency (Eq. (17)). In addition, for $\bar{\beta}_{\text{HS}}$ to be constant, the resonators of the HS must have different stiffness values, since $\beta_{m_{\text{HS}}}$ depends on radius (Eq. (15)). This forces each of the resonators of the HS to also have different moments of inertia to keep their resonance frequencies the same. The LREPC used for this case is the same as for the case of $\bar{\beta}_{\text{LREPC}} = \bar{\beta}_{\text{HS}}$ and $\bar{I}_{\text{LREPC}} = \bar{I}_{\text{HS}}$ (Sec. 3.1.1).

Keeping $\bar{\beta}_{\text{HS}}$ and $\bar{\omega}_{\text{HS}}$ constant results in $\bar{I}_{\text{HS}}$ that varies with radius (Fig. 3(*b*)). $\bar{I}_{\text{HS}}$ asymptotically approaches $\bar{I}_{\text{LREPC}}$ as unit cell number increases (Fig. 3(*b*)) and thus similar to the previous comparison, we expect the last few units of the HS to behave more similarly to those of LREPC compared to the first few units. As we shall see in Sec. 4, this will affect the dynamic effective moment of inertia of each unit cell of the HS. As $r_0/\Delta r$ increases, the difference in $\bar{I}_{\text{HS}}$ and $\bar{I}_{\text{LREPC}}$ becomes smaller (Fig. 3(*b*)). Thus, the HS response approaches that of the LREPC as $r_0/\Delta r$ increases (Fig. 3(*c*)).

In the near field, we observe a different response between the LREPC and HS, even close to the resonator resonance frequency (Figs. 3(*c*) and 3(*d*)). For all $\bar{\beta}$ and $\bar{\omega}$, we observe resonant peaks of the HS inside the band gap range of the LREPC close to both the upper and lower edges of the band gap (Figs. 3(*c*) and 3(*d*)). These resonant peaks seem to penetrate further inside the band gap as stiffness and inertia nondimensional parameters increase (Figs. 3(*di*)–3(*diii*)). For higher nondimensional parameters, there is a peak in HS transmission in the neighborhood of the resonance frequency of the resonator (Fig. (3*diii*)), which is not present for the LREPC. This is clear evidence that the behaviors of the systems are quite different even close to the resonance frequency of the resonators, frequency ranges where these materials are typically designed to work.

Both of these comparisons show that in the near field of sources, the HS transmission is quite different from that of the LREPC. Thus, typical properties of periodic locally resonant systems may not be applicable for the HSs. These transmission results are evidence that to replicate well-known phenomena in periodic locally resonant systems in the near field of sources, one must use an LREPC.

3.2 Comparison Between LRPEC and Homogenous System With Equal Static Torsional Stiffness and Resonators. In both previous comparisons (Sec. 3.1), the resonators of the HS are

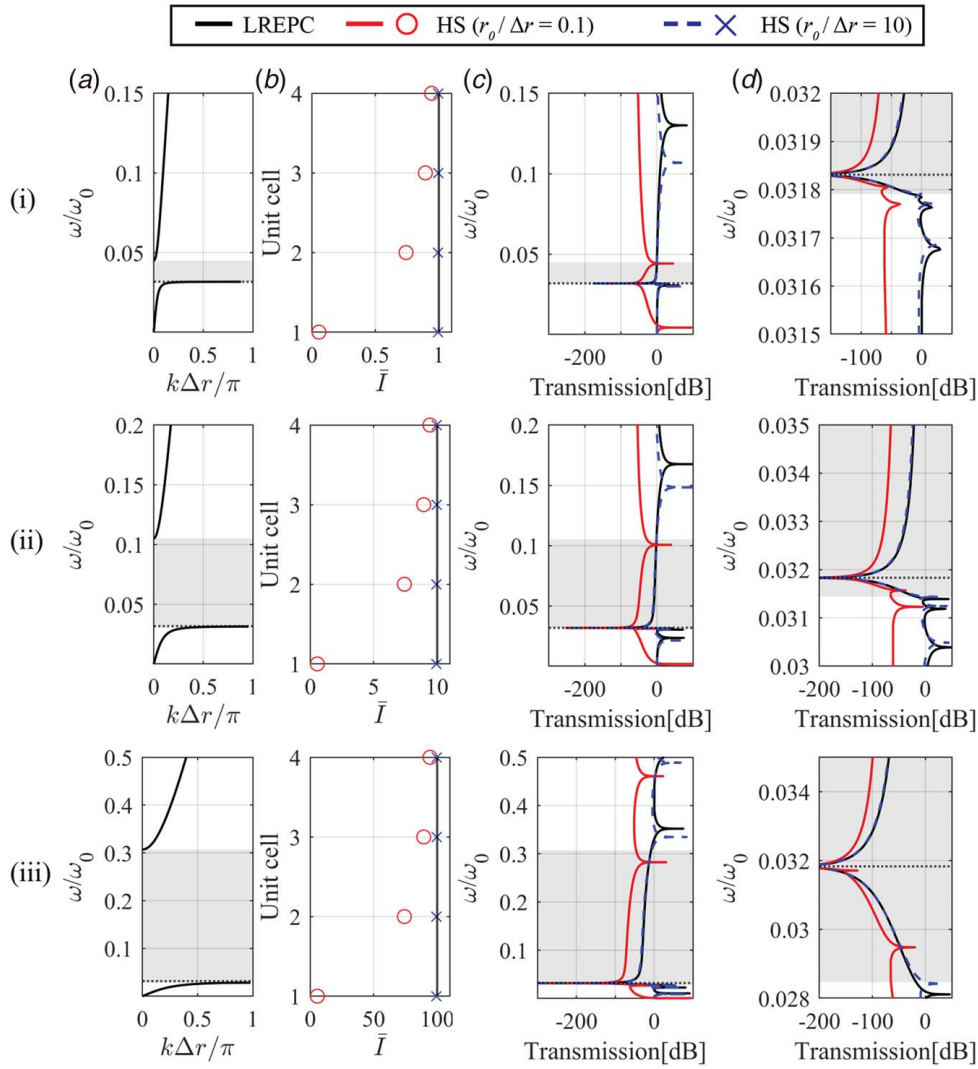

Fig. 3 (*a*) LREPC band structure, (*b*) dependence of $\bar{I}$ on unit cell, (*c*) transmission, and (*d*) zoom in of transmission close to the lower band gap edge of the LREPC. Parameters for each row are as follows: (i) $\bar{\beta}_{\text{LREPC}} = \bar{\beta}_{\text{HS}} = 0.01$ and $\bar{\omega}_{\text{LREPC}} = \bar{\omega}_{\text{HS}} = 0.032$, (ii) $\bar{\beta}_{\text{LREPC}} = \bar{\beta}_{\text{HS}} = 0.1$ and $\bar{\omega}_{\text{LREPC}} = \bar{\omega}_{\text{HS}} = 0.032$, and (iii) $\bar{\beta}_{\text{LREPC}} = \bar{\beta}_{\text{HS}} = 1$ and $\bar{\omega}_{\text{LREPC}} = \bar{\omega}_{\text{HS}} = 0.032$. Black-dotted lines indicate the resonance frequency of the LRPEC resonators.

different in each unit cell. Thus, one might argue that differences in behavior arise from differences in the resonators. In this new case, we aim to compare an LREPC with an HS that has the same resonators, i.e., each resonator has the same stiffness and moment of inertia. To make an accurate comparison, we must somehow relate the stiffnesses and densities of the matrix materials of the LREPC and HS. To do this, we set the static torsional stiffness of both finite systems equal to each other, a possible engineering requirement in the application of these systems.

The objective of this comparison is to study the possible advantages of LREPCs for vibration control applications. When designing a component, there are usually requirements for loading bearing capabilities, for example, a minimum static stiffness. One limitation of locally resonant materials is that the larger the stiffness of the matrix material (which is what carries the load in these systems), the larger the resonator masses and stiffnesses needed for a certain band gap width. This results in more massive systems (in terms of their total mass, i.e., matrix plus resonators) when larger matrix stiffnesses are required, which can be undesirable for performance and cost. So for the final comparison, we compare a four-unit cell LREPC with an HS that has the same quasi-static torsional stiffness and the same resonators.

The static torsional stiffnesses of the finite four-unit cell of the LREPC and the HS are (see Appendix A for more details):

$$\beta_{\text{LREPC}} = \frac{A_0}{r_{\text{out}} - r_0} \tag{18}$$

$$\beta_{\text{HS}} = \frac{2A_{0_{\text{HS}}} r_{\text{out}}^2 r_0^2}{r_{\text{out}}^2 - r_0^2} \tag{19}$$

where $r_{\text{out}} = r_0 + 4\Delta r$, is the outer radius of the finite system. Equating Eqs. (18) and (19) results in,

$$A_{0_{\text{HS}}} = \frac{A_0(r_{\text{out}} + r_0)}{2r_{\text{out}}^2 r_0^2} \tag{20}$$

Note that these equations only define values of $A_{0_{\text{HS}}}$ but not those of $B_{0_{\text{HS}}}$. To define $B_{0_{\text{HS}}}$, we consider that in the limit as $r \to \infty$, both systems should have the same response. This is true if $B_{0_{\text{HS}}} = B_0 A_{0_{\text{HS}}}/A_0$, which is equivalent to setting the shear wave speed of the matrix of the LREPC and HS to be the same.

Interestingly, there is an extra advantage, apart from dynamic effects, of using the LREPC over the HS. For equal quasi-static

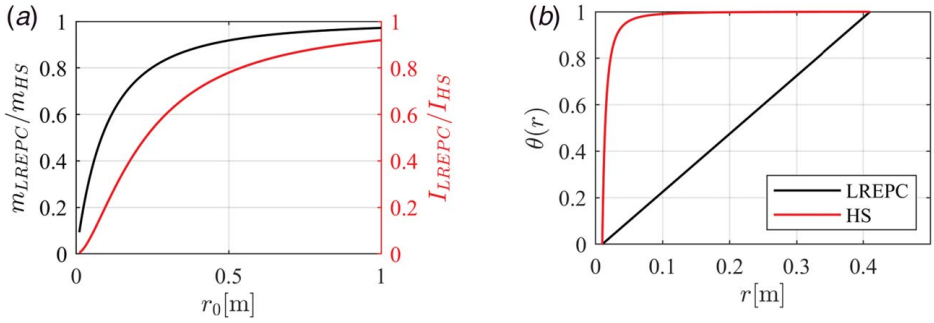

Fig. 4 (*a*) Ratios of mass and moment of inertia of four-unit cell LREPC and HS with equal torsional stiffness and (*b*) static angular displacements of the LREPC and HS with boundary conditions $\theta(r_0 = 0.01) = 0$ and $\theta(r_{out} = r_0 + 4\Delta r = 0.41) = 1$

stiffness and internal radius, the LREPC has both a lower moment of inertia and a lower mass compared to the HS (Fig. (4*a*)) (refer to Appendices B and C for more details). This means that the LREPC uses mass more efficiently. This can be explained by looking at the solution to the quasi-static problem with a fixed internal radius and a prescribed angular displacement on the external radius (Fig. (4*b*)). In the HS, the angular displacements significantly increase with radius at lower radii, while displacements are approximately constant at larger radii. This means that the deformation is concentrated only at very small radii, and most of the material does not deform: This indicates an inefficient distribution of the stiffness and thus of the mass of the matrix of the HS. However, in the LREPC, the angular displacement increases monotonically, meaning the deformation is evenly distributed over the radius. This indicates an efficient distribution of mass, resulting in a lighter system for equal static torsional stiffness. Lower inertia and mass can be advantageous in rotating systems that need to be accelerated and decelerated since they require lower forces and thus lower power to change angular speeds.

Transmissions of LREPC and HS based on this comparison are shown in Fig. 5. As expected, the LREPC transmission has no dependence on $r_0/\Delta r$, and its transmission reduction region agrees well with the one predicted from dispersion (Figs. 5(*a*) and 5(*b*)). Even though all resonators of the HS and the LREPC are the same, their response is still considerably different at lower $r_0/\Delta r$ (Figs. 5(*b*) and 5(*c*)). At low ratios, there are large differences close to the resonator resonance frequencies, where metamaterials support band gaps. Like the HSs from Sec. 3.1, this HS cannot support properties that stem from Bloch analysis.

To further understand the system behaviors, we calculate $\bar{\beta}$, $\bar{I}$, and $\bar{\omega}$ for the HS and the LREPC (Figs. 5(*d*)–5(*f*)). Since resonator frequencies are the same, both systems have the same $\bar{\omega}$; however, $\bar{\beta}$ and $\bar{I}$ are quite different. Contrary to comparisons with equal nondimensional parameters (Sec. 3.1), for a fixed value of $r_0/\Delta r$, $\bar{\beta}_{\rm HS}$ and $\bar{I}_{\rm HS}$ do

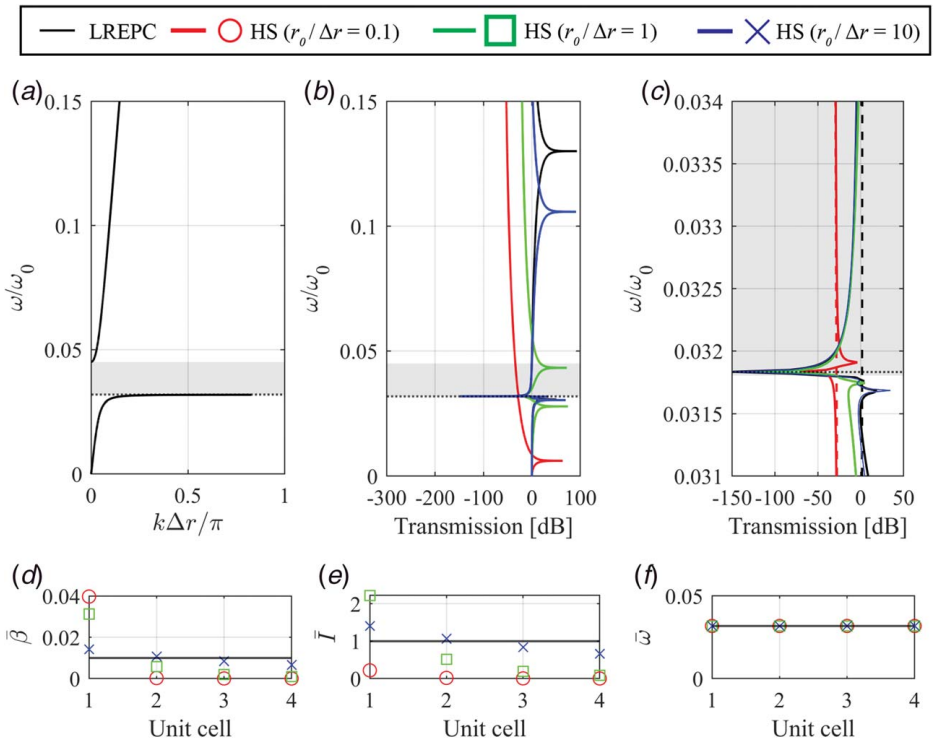

Fig. 5 (*a*) LREPC band structure, (*b*) transmission, (*c*) zoom in of transmission close to the lower band gap edge, (*d*) $\bar{\beta}$, (*e*) $\bar{I}$, and (*f*) $\bar{\omega}$ for each unit cell. Black-dotted lines indicate the resonance frequency of the LREPC and HS resonators. Dashed lines on (c) represent the response of the LREPC and HS system with rigidly attached resonators. For clarity, these are plotted only for the LREPC and the HS with the lower $r_0/\Delta r$.

not asymptotically approximate $\bar{\beta}_{\text{LREPC}}$ and $\bar{I}_{\text{LREPC}}$, respectively, as the unit cell number increases (Figs. 5(*d*) and 3(*e*)). This is because the matrix of the HS becomes stiffer and more massive (in terms of the moment of inertia) as radius increases (Eqs. (15) and (16)). In fact, any HS with equal resonators on all its units will have decreasing $\bar{\beta}_{\text{HS}}$ and $\bar{I}_{\text{HS}}$ as unit cell increases. As shown in Sec. 4, this will affect the effective dynamic properties of this HS system. However, as $r_0/\Delta r$ increases, the HS transmission approximates that of the LRPEC (Fig. (5*c*)). This is because as $r_0/\Delta r$ increases, $\bar{\beta}_{\text{HS}}$, $\bar{I}_{\text{HS}}$, and $\bar{\omega}_{\text{HS}}$ approach $\bar{\beta}_{\text{LREPC}}$, $\bar{I}_{\text{LREPC}}$, and $\bar{\omega}_{\text{LREPC}}$, respectively (Figs. 5(*d*) and 5(*e*)).

To understand the effect of the resonators on each system, we use as reference the transmission for both HS and LREPC when resonators are rigidly attached to the matrix (Fig. 5(*c*)—dashed lines). The reason we do this is so we can normalize for the lower overall transmission due to diffraction in the HS, which is compensated for in the LREPC with the radially dependent matrix material properties. At low $r_0/\Delta r$, only a narrow range of frequencies show differences in transmission of the HS (Fig. 5(*c*)). The effect of the resonators in the transmission of the HS is narrowband compared to the LREPC. This is because of two reasons: (1) the HS has more overall mass and inertia (Fig. 4(*a*)), which is also reflected in $\bar{I}$ values (Fig. 5(*e*)), and (2) the matrix of the HS is softer for low radii but stiffer at larger radii (Fig. 4(*b*)) compared to the matrix of the LREPC, thus, while for the first resonator $\bar{\beta}_{\text{HS}} > \bar{\beta}_{\text{LREPC}}$, the other three show $\bar{\beta}_{\text{HS}} < \bar{\beta}_{\text{LREPC}}$ (Fig. 5(*d*)). Although the masses and stiffnesses of the resonators are the same for LREPC and HS, they produce a smaller effect in the HS and are thus less efficient in affecting response compared to the resonators in the LREPC.

Note that in the locally resonant case, even for $r_0/\Delta r$ as high as 1 (Fig. 5(*b*)), where our previous study on Bragg scattering-based EPCs [22] have shown that the behavior of the EPCs to be quite close to their homogenous counterparts, the transmission of the LREPC and the HS is quite different. This is because the near-field effects are more significant at lower frequencies and lower radii. The Bragg scattering-based EPC requires large unit cells (i.e., larger radii) to obtain low-frequency band gaps. Even if band gaps frequencies in EPCs were lower, most of the structure would still be operating at large radii where near-field effects are not as significant. Instead, in the LREPC, band gap frequencies depend on the resonant frequencies of the resonators and are independent of unit cell size. Thus, low-frequency band gaps can be obtained for metamaterials with small radii where near-field effects are more significant. Note that the band gaps of the LREPC presented here are about 4% of the Bragg frequency (Fig. 5(*a*)).

4 Effective Dynamic Moment of Inertia

Capabilities of locally resonant materials such as negative refraction [20,39], mode conversion [20], and low-frequency vibration absorption [15] arise from their negative effective dynamic properties. Here, we compare the effective dynamic moments of inertia (I_{eff}) of the LREPC and HS as final evidence of how LREPCs can be advantageous for novel wave propagation control in the near field of sources.

I_{eff} for a unit cell is numerically calculated by analyzing its dynamic response to a unit harmonic displacement at its boundary nodes [40]. Under the long wavelength assumption,

$$I_{eff}(\omega) = \frac{\bar{T}(\omega)}{-\omega^2 \theta_{\text{avg}}} \tag{21}$$

where $\bar{T}$ is the resultant torque on the boundary nodes of the unit cell (calculated using Eq. (2)) and θ_{avg} is the average of the angular displacements at the boundary nodes of the unit cell.

Figure 6 shows the frequency ranges of negative I_{eff} of each unit cell of the LREPC and HS for each of the three comparisons (Sec. 3), taking $\frac{r_0}{\Delta r} = 0.1$, $\bar{\beta}_{\text{LREPC}} = 0.01$, and $\bar{I}_{\text{LREPC}} = 1$. Due to its effective periodicity, I_{eff} for all unit cells of the LREPC are the same. Similar to a Cartesian periodic locally resonant system, e.g., Ref. [17], the frequency range of negative I_{eff} of all units of the LREPC align with the band gap frequency range. Because the LREPC is effectively periodic, the negative I_{eff} occurs in the entire system and is independent of radius. On the contrary, the HS equations of motion are not invariant to translations, and thus, each of the HS units will have different dynamic effective properties. In fact, the frequency ranges of negative I_{eff} are different for all HSs studied.

For the case where $\bar{\beta}_{\text{HS}} = \bar{\beta}_{\text{LREPC}}$ and $\bar{I}_{\text{HS}} = \bar{I}_{\text{LREPC}}$ (Sec. 3.1.1), the resonators of the HS all have different resonance frequencies (Fig. 2(*bi*)). The lower bounds of the range of negative I_{eff} of this HS are equal to the resonance frequency of the resonator of each unit cell (Fig. 6(*a*)). As the unit cell number increases, the resonance frequency of the resonators of the HS, and thus, its I_{eff}, approaches that of the LREPC. The range of negative I_{eff} is different for each unit cell, and there is no overlap of ranges between the first unit and the other three units.

The HS where $\bar{\beta}_{\text{HS}} = \bar{\beta}_{\text{LREPC}}$ and $\bar{\omega}_{\text{HS}} = \bar{\omega}_{\text{LREPC}}$(Sec. 3.1.2) also shows differences in the I_{eff} of its unit cells (Fig. 6(*b*)). Since all its resonators have the same resonance frequency (and equal to that of the LREPC), the lower bound of the frequency range of negative I_{eff} for the HS is the same as that of the LREPC. However, these ranges are smaller in the HS compared to the LREPC, particularly in the first few unit cells. This can be explained by looking at the dependence of $\bar{I}_{\text{HS}}$ on unit cell (Fig. 3(*bi*)). In the inner unit cells, $\bar{I}_{\text{HS}}$ are small compared to $\bar{I}_{\text{LREPC}}$, and thus, the I_{eff} becomes negative in a narrower frequency region. In the outer unit cells (approaching the far field), $\bar{I}_{\text{HS}}$ converges to $\bar{I}_{\text{LREPC}}$ and thus so do the I_{eff} of LREPC and HS.

In the HS with equal static torsional stiffness and resonators (Sec. 3.2), all resonators are the same (Fig. 5(*f*)), but the stiffness and moment of inertias of the HS matrix increase with each unit

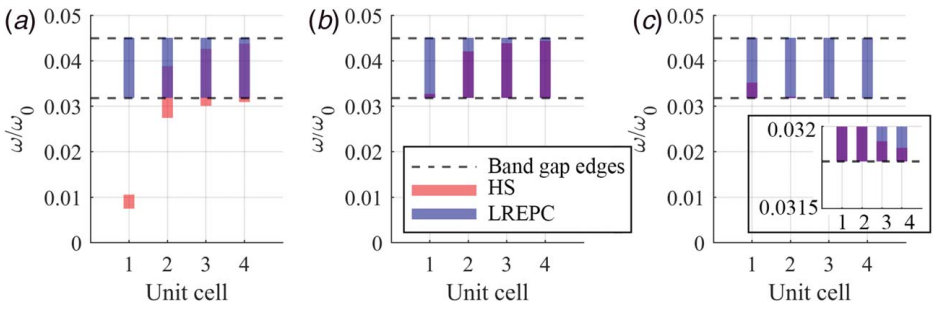

Fig. 6 Frequency ranges of negative effective moment of inertia with $\frac{r_0}{\Delta r} = 0.1$ for (*a*) $\bar{\beta}_{\text{HS}} = \bar{\beta}_{\text{LREPC}} = 0.01$ and $\bar{I}_{\text{HS}} = \bar{I}_{\text{LREPC}} = 1$, (*b*) $\bar{\beta}_{\text{HS}} = \bar{\beta}_{\text{LREPC}} = 0.01$ and $\bar{\omega}_{\text{HS}} = \bar{\omega}_{\text{LREPC}} = 0.032$, and (c) equal static torsional stiffness and resonators with $\bar{\beta}_{\text{LRPEC}} = 0.01$ and $\bar{I}_{\text{LREPC}} = 1$. Inset on (c) shows zoom in view in the neighborhood of the lower band gap edge of the LREPC.

cell (Eqs. (15) and (16)). Thus, $\bar{\beta}_{HS}$ and $\bar{I}_{HS}$ decrease as unit cell increases (Figs. 5(*d*) and 5(*e*)), resulting in a frequency range of negative I_{eff} that decreases as the unit cell increases (Fig. 6(*c*)). In fact, this range becomes almost negligible in the fourth and final unit cells.

This analysis shows that negative effective properties of all the HSs occur over a limited frequency range and also depend on radius. On the contrary, the LREPC behavior is independent of radius, and all its units show a negative effective moment of inertia inside the frequency ranges predicted by its band structure, just like Cartesian metamaterials.

5 Conclusion

In this article, we extend the concept of EPCs [22] to include local resonances, in what we term LREPCs. We show that by using radially varying matrix properties with attached resonators, we can obtain a locally resonant material with equations of motions that are invariant to translations. This allows the application of the Bloch theorem, not only simplifying the analysis but also enabling properties of periodic locally resonant systems in the near field of sources, where plane wave assumptions are not valid.

We compare the behavior of the LREPC to three different HSs that are not "effectively periodic" but instead have geometrically periodic matrix material properties. Because of this, the equations of motion of the HSs are not invariant to translations. For all three cases, the transmission of the LREPC is quite different than the HS, particularly in the near field. This shows that using the LREPC is the only way to realize the typical properties of locally resonant metamaterials for cylindrical wave fronts. To further support this point, we show that the negative I_{eff} of the HS strongly depend on the radius and are limited to small frequency ranges, particularly in the near field. However, frequency ranges of negative I_{eff} of the LREPC are independent of radius and coincide with its band gap frequencies, just like typical Cartesian locally resonant systems.

Interestingly, cylindrical and spherical waves are not the only examples where geometrically periodic systems result in nonperiodic coefficients; for example, this is also the case in periodic pendula. In fact, periodically architected pendula approximate a periodic behavior if a large mass is added at its end, and recent work has shown that a "pseudo" unit cell can be defined from the dynamics of the finite system [41]. Even though there are differences in terms of mathematical approaches and compositions, radial wave crystals [23], EPCs [22] and LREPCs, and periodically architected pendula [41] all have a similar overarching concept: moving away from geometric periodicity and instead defining a mathematically periodic system, thus expanding the boundary of where the Bloch theorem applies. In this way, these studies broaden the concepts of PCs and metamaterials to a new range of mechanical systems.

Our study considers torsional waves and axisymmetric wave propagation, which has applications to rotational machinery or microelectromechanical systems, opening opportunities to embedded wave propagation control mechanisms in waves that propagate outward from a central source or axis. However, similar mathematical treatment could extend these concepts to other wave polarizations and nonaxisymmetric wave propagation. In this way, we can further exploit the platform presented herein to address near-field effects in metamaterials.

Acknowledgment

This material is based upon work supported by the National Science Foundation under Grant No. CMMI-2031110.

Conflict of Interest

There are no conflicts of interest.

Data Availability Statement

The datasets generated and supporting the findings of this article are obtainable from the corresponding author upon reasonable request. The authors attest that all data for this study are included in the paper.

Funding Data

- National Science Foundation (NSF) (Grant No. CMMI-2031110; Funder ID: 10.13039/501100008982).

Nomenclature

h = out-of-plane thickness
A = matrix stiffness function LREPC
B = matrix density function LREPC
I = polar mass moment of inertia
M = external moment
T = torque
$\bar{I}$ = moment of inertia nondimensional parameter
r_0 = inner radius
r_{out} = outer radius
u_θ = tangential displacements
A_0 = matrix stiffness constant of LREPC
A_{0HS} = matrix stiffness constant of HS
B_0 = matrix density constant of LREPC
B_{0HS} = matrix density constant of HS
I_{eff} = effective dynamic moment of inertia
I_r = polar mass moment of inertia of the resonators
$\bar{I}_{HS}$ = moment of inertia nondimensional parameter of the HS
$\bar{I}_{LREPC}$ = moment of inertia nondimensional parameter of the LREPC
β_r = torsional stiffness of resonators
β_{HS} = static torsional stiffness of four-unit cell HS
β_{LREPC} = static torsional stiffness of four-unit cell LREPC
$\bar{\beta}$ = stiffness nondimensional parameter
$\bar{\beta}_{HS}$ = stiffness nondimensional parameter of the HS
$\bar{\beta}_{LREPC}$ = stiffness nondimensional parameter of the LREPC
Δr = periodicity constant
θ = angular displacement
μ = shear modulus
ρ = density
$\sigma_{r\theta}$ = shear stress
ω = angular frequency

Appendix A: Static Stiffness of LREPC and Homogenous System

Static torsional stiffness of LREPC and HS finite systems, as well as their unit cells, are calculated by solving the boundary value problem arising from Eq. (6), neglecting inertial effects and imposing angular displacements in both inner and outer ring surfaces:

$$\begin{cases} \dfrac{\partial}{\partial r}\left(r^3 A(r)\dfrac{\partial \theta}{\partial r}\right) = 0 \\ \theta(r_{in}) = \theta_1 \\ \theta(r_{out}) = \theta_2 \end{cases} \tag{A1}$$

We substitute material properties for the LREPC (Eq. (7)) and the HS (Eq. (14)) and solve for $\theta(r)$. We define the static torsional stiffness as follows:

$$\beta = \frac{T(r_{out})}{\theta_2 - \theta_1} \tag{A2}$$

where $T(r)$ is the moment as defined in Eq. (3). We replace r_{out} and r_{in} by inner and outer radii of the unit cell, respectively, and by r_0 and $r_0 + N\Delta r$ for static stiffness of the unit cells and systems of N unit cells, respectively.

Appendix B: Polar Mass Moment of Inertia of LREPC and Homogenous System

Moment of inertia of LREPC and HS systems as well as their unit cells are calculated as follows:

$$\int_{\Omega} \rho(r) r^2 dV = \int_{r_{in}}^{r_{out}} \int_{0}^{2\pi} \int_{0}^{h(r)} \rho(r) r^3 dr d\theta dz = 2\pi \int_{r_{in}}^{r_{out}} \rho(r) h(r) r^3 dr$$
$$= 2\pi \int_{r_{in}}^{r_{out}} B(r) r^3 dr \tag{B1}$$

We substitute material properties for the LREPC (Eq. (7)) and the HS (Eq. (14)) and replace r_{out} and r_{in} by inner and outer radii of the unit cell and by r_0 and $r_0 + N\Delta r$ for the moment of inertia of the unit cells and systems of N unit cells, respectively.

Appendix C: Mass of LREPC and Homogenous System

Mass of LREPC and HS systems are follows:

$$\int_{\Omega} \rho(r) dV = \int_{r_0}^{r_0+N\Delta r} \int_{0}^{2\pi} \int_{0}^{h(r)} \rho(r) r dr d\theta dz = 2\pi \int_{r_0}^{r_0+N\Delta r} \rho(r) h(r) r dr$$
$$= 2\pi \int_{r_0}^{r_0+N\Delta r} B(r) r dr \tag{C1}$$

We substitute material properties for the LREPC (Eq. (7)) and the HS (Eq. (14)) and replace r_{out} and r_{in} by inner and outer radii of the unit cell and by r_0 and $r_0 + N\Delta r$ for the mass of the unit cells and whole systems, respectively.

References

[1] Hussein, M. I., Leamy, M. J., and Ruzzene, M., 2014, "Dynamics of Phononic Materials and Structures: Historical Origins, Recent Progress, and Future Outlook," ASME Appl. Mech. Rev., **66**(4), p. 040802.

[2] Khelif, A., and Adibi, A., 2015, *Phononic Crystals: Fundamentals and Applications*, Springer, New York.

[3] Sigalas, M., and Economou, E. N., 1993, "Band Structure of Elastic Waves in Two Dimensional Systems," Solid State Commun., **86**(3), pp. 141–143.

[4] Matlack, K. H., Bauhofer, A., Krödel, S., Palermo, A., and Daraio, C., 2016, "Composite 3D-Printed Metastructures for Low-Frequency and Broadband Vibration Absorption," Proc. Natl. Acad. Sci., **113**(30), pp. 8386–8390.

[5] Pierce, C. D., Willey, C. L., Chen, V. W., Hardin, J. O., Berrigan, J. D., Juhl, A. T., and Matlack, K. H., 2020, "Adaptive Elastic Metastructures From Magneto-Active Elastomers," Smart Mater. Struct., **29**(6), p. 065004.

[6] Nimmagadda, C., and Matlack, K. H., 2019, "Thermally Tunable Band Gaps in Architected Metamaterial Structures," J. Sound Vib., **439**, pp. 29–42.

[7] Bertoldi, K., 2017, "Harnessing Instabilities to Design Tunable Architected Cellular Materials," Annu. Rev. Mater. Res., **47**(1), pp. 51–61.

[8] Yang, S., Page, J. H., Liu, Z., Cowan, M. L., Chan, C. T., and Sheng, P., 2004, "Focusing of Sound in a 3D Phononic Crystal," Phys. Rev. Lett., **93**(2), p. 024301.

[9] Sukhovich, A., Merheb, B., Muralidharan, K., Vasseur, J. O., Pennec, Y., Deymier, P. A., and Page, J. H., 2009, "Experimental and Theoretical Evidence for Subwavelength Imaging in Phononic Crystals," Phys. Rev. Lett., **102**(15), p. 154301.

[10] Süsstrunk, R., and Huber, S. D., 2015, "Observation of Phononic Helical Edge States in a Mechanical Topological Insulator," Science, **349**(6243), pp. 47–50.

[11] Mousavi, S. H., Khanikaev, A. B., and Wang, Z., 2015, "Topologically Protected Elastic Waves in Phononic Metamaterials," Nat. Commun., **6**(1), pp. 1–7.

[12] Wang, P., Lu, L., Bertoldi, K., John, H., and Paulson, A., 2015, "Topological Phononic Crystals With One-Way Elastic Edge Waves," Phys. Rev. Lett., **115**(10), p. 104302.

[13] Wang, Y.-T., Luan, P.-G., and Zhang, S., 2015, "Coriolis Force Induced Topological Order for Classical Mechanical Vibrations Related Content," New J. Phys., **17**(7), p. 073031.

[14] Brillouin, L., 1946, *Wave Propagation in Periodic Structures; Electric Filters and Crystal Lattices*, McGraw-Hill, New York.

[15] Liu, Z., Zhang, X., Mao, Y., Zhu, Y. Y., Yang, Z., Chan, C. T., and Sheng, P., 2000, "Locally Resonant Sonic Materials," Science, **289**(5485), pp. 1734–1736.

[16] Hussein, M. I., and Frazier, M. J., 2013, "Metadamping: An Emergent Phenomenon in Dissipative Metamaterials," J. Sound Vib., **332**(20), pp. 4767–4774.

[17] Huang, H. H., Sun, C. T., and Huang, G. L., 2009, "On the Negative Effective Mass Density in Acoustic Metamaterials," Int. J. Eng. Sci., **47**(4), pp. 610–617.

[18] Den Hartog, J. P., 1947, *Mechanical Vibrations*, McGraw-Hill Book Compnay, Inc., New York.

[19] Christensen, J., and García De Abajo, F. J., 2012, "Anisotropic Metamaterials for Full Control of Acoustic Waves," Phys. Rev. Lett., **108**(12), p. 124301.

[20] Zhu, R., Liu, X. N., Hu, G. K., Sun, C. T., and Huang, G. L., 2014, "Negative Refraction of Elastic Waves at the Deep-Subwavelength Scale in a Single-Phase Metamaterial," Nat. Commun., **5**(1), p. 5510.

[21] Ge Kaina, N., Lemoult, F., Fink, M., and Lerosey, G., 2015, "Negative Refractive Index and Acoustic Superlens From Multiple Scattering in Single Negative Metamaterials," Nature, **525**(7567), pp. 77–81.

[22] Arretche, I., and Matlack, K. H., 2020, "Effective Phononic Crystals for Non-Cartesian Elastic Wave Propagation," Phys. Rev. B, **102**(13), p. 134308.

[23] Torrent, D., and Sánchez-Dehesa, J., 2009, "Radial Wave Crystals: Radially Periodic Structures From Anisotropic Metamaterials for Engineering Acoustic or Electromagnetic Waves," Phys. Rev. Lett., **103**(6), p. 064301.

[24] Hvatov, A., and Sorokin, S., 2018, "On Application of the Floquet Theory for Radially Periodic Membranes and Plates," J. Sound Vib., **414**, pp. 15–30.

[25] Haisheng, S., Liqiang, D., Shidan, L., Wei, L., Shaogang, L., Weiyuan, W., Dongyan, S., and Dan, Z., 2014, "Propagation of Torsional Waves in a Thin Circular Plate of Generalized Phononic Crystals," J. Phys. D: Appl. Phys., **47**(29), p. 295501.

[26] Yeh, P., Yariv, A., and Maron, E., 1978, "Theory of Bragg Fiber," J. Opt. Soc. Am., **68**(9), pp. 1196–1201.

[27] Shu, H., Zhao, L., Shi, X., Liu, W., Shi, D., and Kong, F., 2015, "Torsional Wave Propagation in a Circular Plate of Piezoelectric Radial Phononic Crystals," J. Appl. Phys., **118**(18), p. 184904.

[28] Xu, Z., Wu, F., and Guo, Z., 2012, "Low Frequency Phononic Band Structures in Two-Dimensional Arc-Shaped Phononic Crystals," Phys. Lett. A, **376**(33), pp. 2256–2263.

[29] Ma, T., Chen, T., Wang, X., Li, Y., and Wang, P., 2014, "Band Structures of Bilayer Radial Phononic Crystal Plate With Crystal Gliding," J. Appl. Phys., **116**(10), p. 104505.

[30] Xiao, Y., Mace, B. R., Wen, J., and Wen, X., 2011, "Formation and Coupling of Band Gaps in a Locally Resonant Elastic System Comprising a String With Attached Resonators," Phys. Lett. A, **375**(12), pp. 1485–1491.

[31] Wang, G., Wen, X., Wen, J., and Liu, Y., 2006, "Quasi-One-Dimensional Periodic Structure With Locally Resonant Band Gap," ASME J. Appl. Mech., **73**(1), pp. 167–170.

[32] Wachel, J. C., and Szenasi, F. R., 1993, "Analysis of Torsional Vibrations in Rotating Machinery," Proceedings of the Twenty-Second Turbomachinery Symposium, Dallas, TX, Sept. 14–16, pp. 127–151.

[33] Ma, G., Fu, C., Wang, G., Del Hougne, P., Christensen, J., Lai, Y., and Sheng, P., 2016, "Polarization Bandgaps and Fluid-Like Elasticity in Fully Solid Elastic Metamaterials," Nat. Commun., **7**(1), pp. 1–8.

[34] Yu, D., Liu, Y., Wang, G., Cai, L., and Qiu, J., 2006, "Low Frequency Torsional Vibration Gaps in the Shaft With Locally Resonant Structures," Phys. Lett. A, **348**(3–6), pp. 410–415.

[35] Ma, G., and Sheng, P., 2016, "Acoustic Metamaterials: From Local Resonances to Broad Horizons," Sci. Adv., **2**(2), p. e1501595.

[36] Yu, D., Liu, Y., Wang, G., Zhao, H., and Qiu, J., 2006, "Flexural Vibration Band Gaps in Timoshenko Beams With Locally Resonant Structures," J. Appl. Phys., **100**(12), p. 124901.

[37] Nouh, M. A., Aldraihem, O. J., and Baz, A., 2016, "Periodic Metamaterial Plates With Smart Tunable Local Resonators," J. Intell. Mater. Syst. Struct., **27**(13), pp. 1829–1845.

[38] Krödel, S., Thomé, N., and Daraio, C., 2015, "Wide Band-Gap Seismic Metastructures," Extreme Mech. Lett., **4**, pp. 111–117.

[39] Wu, Y., Lai, Y., and Zhang, Z.-Q., 2011, "Elastic Metamaterials With Simultaneously Negative Effective Shear Modulus and Mass Density," Phys. Rev. Lett., **107**(10), p. 124901.

[40] Liu, X. N., Hu, G. K., Sun, C. T., and Huang, G. L., 2011, "Wave Propagation Characterization and Design of Two-Dimensional Elastic Chiral Metacomposite," J. Sound Vib., **330**(11), pp. 2536–2553.

[41] Al Ba'ba'a, H., Callanan, J., and Nouh, M., 2019, "Emergence of Pseudo-Phononic Gaps in Periodically Architected Pendulums," Front. Mater., **6**, p. 119.